Atmos. Chem. Phys. Discuss., https://doi.org/10.5194/acp-2017-1183
Manuscript under review for journal Atmos. Chem. Phys.
Discussion started: 12 February 2018

Atmospheric Chemistry and Physics Discussions

Insight into Global Trends in Aerosol Composition over 2005-2015 Inferred from the OMI Ultraviolet Aerosol Index

Melanie S. Hammer[1], Randall V. Martin[1,2], Chi Li[1], Omar Torres[3], Max Manning[1], Brian L. Boys[1]

[1]Department of Physics and Atmospheric Science, Dalhousie University, Canada
[2]Harvard-Smithsonian Center for Astrophysics, Cambridge, MA, USA
[3]Atmospheric Chemistry and Dynamics Laboratory, NASA Goddard Space Flight Center, Greenbelt, MD, 20770, USA

Correspondence: melanie.hammer@dal.ca

Abstract

Observations of aerosol scattering and absorption offer valuable information about aerosol composition. We apply a simulation of the Ultraviolet Aerosol Index (UVAI), a method of detecting aerosol absorption from satellite observations, to interpret UVAI values observed by the Ozone Monitoring Instrument (OMI) over 2005-2015 to understand global trends in aerosol composition. We conduct our simulation using the vector radiative transfer model VLIDORT with aerosol fields from the global chemical transport model GEOS-Chem. We examine the 2005-2015 trends in individual aerosol species from GEOS-Chem, and apply these trends to the UVAI simulation to calculate the change in simulated UVAI due to the trends in individual aerosol species. We find that global trends in the UVAI are largely explained by trends in absorption by mineral dust, absorption by brown carbon, and scattering by secondary inorganic aerosol. Trends in absorption by mineral dust dominate the simulated UVAI trends over North Africa, the Middle-East, East Asia, and Australia. The UVAI simulation well resolves observed negative UVAI trends over Australia, but underestimates positive UVAI trends over North Africa and Central Asia near the Aral Sea, and underestimates negative UVAI trends over East Asia. We find evidence of an increasing dust source from the desiccating Aral Sea, that may not be well represented by the current generation of models. Trends in absorption by brown carbon dominate the simulated UVAI trends over biomass burning regions. The UVAI simulation reproduces observed negative trends over central South America and West Africa, but underestimates observed UVAI trends over boreal forests. Trends in scattering by secondary inorganic aerosol dominate the simulated UVAI

Atmos. Chem. Phys. Discuss., https://doi.org/10.5194/acp-2017-1183
Manuscript under review for journal Atmos. Chem. Phys.
Discussion started: 12 February 2018

trends over the eastern United States and eastern India. The UVAI simulation slightly overestimates the observed positive UVAI trends over the eastern United States, and underestimates the observed negative UVAI trends over India. Quantitative simulation of the OMI UVAI offers new insight into global trends in aerosol composition.

1. Introduction

Atmospheric aerosols have significant climate impacts due to their ability to scatter and absorb solar radiation. The exact magnitude of the direct radiative forcing remains highly uncertain (IPCC, 2014), although most studies agree it is significant (Andreae and Gelencsér, 2006; Mann and Emanuel, 2006; Mauritsen, 2016). Storelvmo et al. (2016) estimate that changes in global aerosol loading over the past 45 years have caused cooling (direct and indirect) that masks about one third of the atmospheric warming due to increasing greenhouse gas emissions. Aerosol absorption has been estimated to be the second largest source of atmospheric warming after carbon dioxide (Ramanathan and Carmichael, 2008; Bond et al., 2013; IPCC, 2014), although considerable uncertainty remains regarding the exact magnitude (Stier et al., 2007). The large uncertainty regarding the direct radiative impacts of aerosols on climate is driven by the large variability in aerosol physical and chemical properties, as well as their various emission sources, making it extremely difficult to fully understand their interactions with radiation (Pöschl, 2005; Moosmüller et al., 2009; Curci et al., 2015; Kristiansen et al., 2016). Global observations of trends in aerosol scattering and absorption would offer valuable constraints on trends in aerosol sources and composition.

The emissions of aerosols and their precursors have changed significantly over the past decade. In North America and Europe, the anthropogenic emissions of most aerosol species (e.g. black carbon, organic aerosols) and aerosol precursors (e.g. sulfur dioxide and nitrogen oxides) have decreased due to pollution controls (Leibensperger et al., 2012; Klimont et al., 2013; Curier et al., 2014; Simon et al., 2014; Xing et al., 2015; Li et al., 2017a). By contrast, emissions of aerosols and aerosol precursors have increased in developing countries due to increased industrial activity, particularly in China and India. Chinese emissions of black carbon (BC), organic carbon (OC), and nitrogen oxides (NO_x) have been increasing over the past decade (Zhao et al., 2013; Cui et al., 2015), although in the most recent years NO_x emissions have been declining, driven by denitration devices at power plants (Liu et al., 2016). Due to the wide implementation of flue-gas

desulfurization equipment on most power plants in China, emissions of sulfur dioxide (SO_2) in some regions have been decreasing since about 2006-2008 (Lu et al., 2011; Wang et al., 2015). Indian emissions of anthropogenic aerosols and their precursors have been increasing over the past decade (Lu et al., 2011; Klimont et al., 2017). There have also been significant changes in global dust and biomass burning emissions. Shao et al. (2013) use synoptic data to estimate a global decrease in dust emissions between 1974 and 2012, driven largely by reductions from North Africa with weaker contributions from Northeast Asia, South America, and South Africa. By examining trends in burned area, Giglio et al. (2013) estimate a decrease in global biomass burning emissions between 2000 and 2012. Trends in aerosol composition produced by these changing emissions may be detectable from satellite observations of aerosol scattering and absorption.

Detection of aerosol composition from passive nadir satellite observations is exceedingly difficult; few methods exist. The aerosol-type classification provided by retrievals from the MISR instrument, enabled by multi-angle viewing, is one such source of information about aerosol composition from constraints on particle size, shape, and single scattering albedo (SSA) (Kahn and Gaitley, 2015). MISR retrievals have been used to classify particles relating to events such as biomass burning, desert dust, volcanic eruptions, and pollution events (e.g. Liu et al., 2007; Kalashnikova and Kahn, 2008; Dey and Di Girolamo, 2011; Scollo et al., 2012; Guo et al., 2013). The most commonly used satellite product for aerosol information is aerosol optical depth (AOD), the columnar extinction of radiation by atmospheric aerosols. AOD can be retrieved from satellite measurements of top of atmosphere radiance in combination with prior knowledge of aerosol optical properties. Several studies have examined trends in satellite AOD. Following trends in emissions, over the past decade positive trends in satellite AOD have been observed over Asia and Africa corresponding to regions experiencing industrial growth (de Meij et al., 2012; Chin et al., 2014a; Mao et al., 2014; Mehta et al., 2016), while negative trends in satellite AOD have been observed over North America and Europe, largely due to pollution controls (Hsu et al., 2012; de Meij et al., 2012; Chin et al., 2014b; Mehta et al., 2016). Studies such as these demonstrate the information about the evolution of aerosol abundance offered by total column AOD retrievals, however measurements of absorption would complement the information in AOD retrievals by providing independent information on aerosol composition.

The Ultraviolet Aerosol Index (UVAI) is a method of detecting aerosol absorption from satellite measured radiances (Herman et al., 1997; Torres et al., 1998). Because the UVAI is

calculated from measured radiances, a priori assumptions about aerosol composition are not required for its calculation, thus yielding independent information on aerosol scattering and absorption. The UVAI has been widely applied to examine mineral dust (Israelevich et al., 2002; Schepanski et al., 2007; Badarinath et al., 2010; Huang et al., 2010) and biomass burning aerosols (Duncan et al., 2003; Guan et al., 2010; Torres et al., 2010; Kaskaoutis et al., 2011; Mielonen et al., 2012), including brown carbon (Jethva and Torres, 2011; Hammer et al., 2016). The UVAI is not typically used to examine scattering aerosol, however aerosol scattering causes a net decrease in the UVAI, meaning that the UVAI could be used to detect changes due to both aerosol absorption and scattering. Prior interpretation of the UVAI has been complicated by its dependence on other parameters, such as aerosol layer height. Examining trends in the UVAI would provide an exciting opportunity to investigate the evolution of aerosol absorption and scattering over time, if the multiple parameters affecting the UVAI could be accounted for through simulation.

In this work, we apply a simulation of the UVAI, which was developed and evaluated in Hammer et al. (2016), to interpret trends in recently reprocessed OMI UVAI observations for 2005-2015 to understand global changes in aerosol composition. We interpret observed UVAI values by using a radiative transfer model (VLIDORT) to calculate UVAI values as a function of simulated aerosol composition from the global 3-D chemical transport model GEOS-Chem. Comparison of trends in observed OMI UVAI values to the trends in simulated UVAI values, which are calculated using known aerosol composition, enables qualification of how changes in aerosol absorption and scattering could influence the observed UVAI trends. Section 2 describes the OMI UVAI observations and our UVAI simulation. Section 3 examines the trends in emissions of GEOS-Chem aerosols and their precursors for 2005-2015 to provide context for the trends in our simulated UVAI. Section 4 compares the mean values over 2005-2015 of the OMI UVAI and our simulated UVAI. Section 5 compares the 2005-2015 trends in OMI and simulated UVAI values. In section 6 we examine the sensitivity of the UVAI to changes in the abundance of individual aerosol species. Trends in our UVAI simulation are interpreted by applying the trends in the GEOS-Chem aerosol species to calculate the associated change in UVAI. Section 7 reports the conclusions.

Atmos. Chem. Phys. Discuss., https://doi.org/10.5194/acp-2017-1183
Manuscript under review for journal Atmos. Chem. Phys.
Discussion started: 12 February 2018

2. Methods

2.1 OMI Ultraviolet Aerosol Index

The OMI Ultraviolet Aerosol Index is a method of detecting absorbing aerosols from satellite measurements in the near-UV wavelength region and is a product of the OMI Near-UV algorithm (OMAERUV) (Torres et al., 2007). The OMAERUV algorithm uses the 354 nm and 388 nm radiances measured by OMI to calculate the UVAI as a measure of the deviation from a purely Rayleigh scattering atmosphere bounded by a Lambertian reflecting surface. Positive UVAI values indicate absorbing aerosol while negative values indicate non-absorbing aerosol. Near-zero values occur when clouds and Rayleigh scattering dominate. Negative UVAI values due to aerosol scattering are often weak and buried in noise (Torres et al., 2007). Because UVAI values are calculated from top of atmosphere (TOA) radiance which contains total aerosol effects, the presence (or lack) of scattering aerosol along with absorbing aerosol will either weaken (or strengthen) the absorption signal. Therefore the UVAI could be used to detect changes over time due to both aerosol absorption and scattering.

The OMAERUV algorithm also produces retrieved OMI single scattering albedo (SSA) and AOD derived from the observed radiances, aerosol type selection using the OMI UVAI, AIRS carbon monoxide, and aerosol layer height assumptions constrained by climatologies from CALIOP retrievals and a GOCART simulation. These OMI SSA and AOD products have been subjected to rigorous validation studies and have been found to be in reasonable agreement with independent ground-based AOD and SSA inferred from AERONET measurements (Torres et al., 2007, 2013; Ahn et al., 2014; Jethva et al., 2014; Zhang et al., 2016). We focus on the UVAI here since simulation of the UVAI product does not require external information from other satellites or models, and thus enables us to isolate information on aerosol composition.

In this analysis, we use a recently reprocessed version of the UVAI algorithm which treats clouds with a Mie-scattering based water cloud model (Torres et al., 2017). This new dataset more accurately accounts for scattering by mineral dust and by clouds, reducing systematic artifacts and scan angle bias. We focus on cloud-filtered observations by excluding scenes with cloud fraction exceeding 0.05. Since 2008 the OMI observations have been affected by a row anomaly which reduces the sensor viewing capability for specific scan angles (http://projects.knmi.nl/omi/research/product/rowanomaly-background.php). The sudden suppression of observations for specific viewing geometries (i.e. the row anomaly), could cause an additional spurious trend in the

UVAI calculation. We reduce this concern by using the recently reprocessed OMAERUV UVAI that is insensitive to scan-angle dependent cloud artifacts and by considering only scan positions 3-23 which remain unaffected by the row anomaly. The monthly time series data are deseasonalized by subtracting the monthly mean for the period 2005-2015. A minimum temporal coverage of 60% is also applied prior to regression. We perform trend analysis on monthly mean time series data for the years 2005-2015 using Generalized Least Squares (GLS) regression, as described by Boys et al. (2014). An additional small, positive, spurious trend in the cloud-filtered OMI UVAI remains which is believed to be due to instrumental effects (Torres et al., 2017). We subtract this spurious global mean trend in the cloud-filtered UVAI prior to interpretation. In the following section, we discuss our UVAI simulation and the implementation of the new UVAI algorithm in the simulation.

2.2 Simulated UVAI

We simulate the UVAI using the VLIDORT radiative transfer model (Spurr, 2006), following Buchard et al. (2015) and Hammer et al. (2016). We calculate the top of atmosphere radiances at 354 nm and 388 nm needed for the UVAI calculation by supplying VLIDORT with the OMI viewing geometry for each scene, as well as the GEOS-Chem simulation of vertical profiles of aerosol extinction, spectrally dependent single scattering albedo, and the corresponding spectrally dependent scattering phase function. Thus these parameters account for the sensitivity of the UVAI to aerosol layer height and spectrally dependent aerosol optical properties.

We introduce to the UVAI simulation a Mie-scattering based water cloud model (Deirmendjian, 1964) for consistency with the reprocessed OMI UVAI dataset. Following Torres et al. (2017), we compute the radiances used in the UVAI calculation as a combination of clear and cloudy sky conditions. We use the same cloud fractions and cloud optical depths used in the OMI UVAI algorithm for coincident OMI pixels. We avoid cloudy scenes by considering only pixels with a cloud fraction of less than 0.05.

We use the GEOS-Chem model v11-01 (http://geos-chem.org) as input to the UVAI simulation, and to calculate the sensitivity of the UVAI simulation to aerosol composition. The simulation is driven by assimilated meteorological data from MERRA-2 Reanalysis of the NASA Global Modeling and Assimilation Office (GMAO). Our simulation is conducted at a spatial

resolution of 2° x 2.5° with 47 vertical levels for the years 2005-2015. We supply VLIDORT with GEOS-Chem aerosol fields coincident with OMI observations.

GEOS-Chem contains a detailed oxidant-aerosol chemical mechanism (Bey et al., 2001; Park et al., 2004). The aerosol simulation includes the sulfate-nitrate-ammonium system (Fountoukis and Nenes, 2007; Park et al., 2004; Pye et al., 2009), primary carbonaceous aerosol (Park et al., 2003), mineral dust (Fairlie et al., 2007), and sea salt (Jaeglé et al., 2011). Semivolatile primary organic carbon and secondary organic aerosol formation is described in Pye et al. (2010). We update the original semi-volatile partitioning of secondary OA (SOA) formed from isoprene with the irreversible uptake scheme in Marais et al. (2016). HNO_3 concentrations are reduced following Heald et al. (2012). Aerosol optical properties are based on the Global Aerosol Data Set (GADS) (Koepke et al., 1997) as originally implemented by Martin et al. (2003), with updates for organics and secondary inorganics from aircraft observations (Drury et al., 2010), for mineral dust (Lee et al., 2009; Ridley et al., 2012), and for absorbing brown carbon (Hammer et al., 2016). Here we update the mineral dust optics at ultraviolet wavelengths using a refractive index that minimizes the difference between the mean simulated and OMI UVAI values to allow focus on trends. Aerosols are treated as externally mixed.

Anthropogenic emissions are from the EDGARv4.3.1 global inventory (Crippa et al., 2016) with emissions overwritten in areas with regional inventories for the United States (NEI11;Travis et al., 2016), Canada (CAC), Mexico (BRAVO; Kuhns et al., 2005), Europe (EMEP; http://www.emep.int/), China (MEIC v1.2; Li et al., 2017a) and elsewhere in Asia (MIX; Li et al., 2017a). Emissions from open fires for individual years from the GFED4 inventory (Giglio et al., 2013) are included. The long-term concentrations from this simulation have been extensively evaluated versus ground-based $PM_{2.5}$ composition measurements where available, and versus satellite-derived $PM_{2.5}$ trends (Li et al., 2017b).

The Supplement evaluates trends in simulated SO_2, NO_2, and AOD versus satellite retrievals from multiple instruments and algorithms. We find broad consistency between our simulated NO_2 and SO_2 column trends with those from OMI (Figures S1 and S2). Our simulated AOD trends are generally consistent with the trends in satellite AOD retrievals, except for positive trends in AOD over western North America and near the Aral Sea in most retrieval products, and a negative trend in AOD over Mongolia/Inner Mongolia in all retrieval products (Figure S3).

Atmos. Chem. Phys. Discuss., https://doi.org/10.5194/acp-2017-1183
Manuscript under review for journal Atmos. Chem. Phys.
Discussion started: 12 February 2018

We filter our GEOS-Chem aerosol simulated fields based on the coincident OMI pixels, which are regridded to the model resolution of 2° x 2.5°. This allows for the direct comparison between our GEOS-Chem simulation and the OMI UVAI observations.

3. Trend in emissions of GEOS-Chem aerosols and their precursors

Figure 1 shows the trends in emissions of aerosols and their precursors from our GEOS-Chem simulation calculated from the GLS regression of monthly time series values for 2005-2015. Cool colors indicate negative trend values, warm colors indicate positive trend values, and the opacity of the colors indicates the statistical significance of the trends. The trends in emissions of sulfur dioxide (SO_2) and nitrogen oxides (NO_x) follow similar patterns (Figure 1a and 1b, respectively). Negative trends of –1 to -0.01 kg km^{-2} yr^{-1} are present over North America and Europe, corresponding to pollution controls (Leibensperger et al., 2012; Klimont et al., 2013; Curier et al., 2014; Simon et al., 2014; Xing et al., 2015; Li et al., 2017a). Positive trends of 0.5 to 1 kg km^{-2} yr^{-1} in both species are present over India and eastern China, however the positive trends in emissions of SO_2 over eastern China are interspersed with negative trends in SO_2 emissions of -1 to -0.5 kg km^{-2} yr^{-1}, corresponding to the deployment of desulfurization equipment on power plants in recent years (Lu et al., 2011; Klimont et al., 2013; Wang et al., 2015). Ammonia (NH_3) emissions (Figure 1c) have positive trends of 0.001 to 0.05 kg km^{-2} yr^{-1} over most of South America, North Africa, the Middle-East, and most of Asia with larger trends of 0.1 to 0.5 kg km^{-2} yr^{-1} over India and eastern China. There are positive trends of 0.001 to 0.05 kg km^{-2} yr^{-1} in black carbon (BC) emissions (Figure 1d) over North Africa, Europe, the Middle-East, India, and China, and negative trends of -0.05 to -0.001 kg km^{-2} yr^{-1} over North America, Europe, West Africa, and central South America. The trends in primary organic aerosol (POA) emissions (Figure 1e) follow a similar pattern as the trends in BC emissions, except there are negative trends over eastern China of -0.1 to -0.05 kg km^{-2} yr^{-1} and the negative trends over West Africa and central South America are larger in magnitude (-1 to -0.1 kg km^{-2} yr^{-1}). Chen et al. (2013) found a significant decreasing trend over 2001-2012 using MODIS data in active fires over central South America due to deforestation in Brazil. Using MODIS fire data, Andela and van der Werf (2014) found a declining trend over 2001-2012 in burned area due to cropland expansion over West Africa. There are also positive trends of 0.001 to 0.05 kg km^{-2} yr^{-1} over the northern United States and Canada. The trends in dust emissions (Figure 1f) show the largest magnitude of all the various species, although many

247 have low statistical significance, with areas of positive and negative trends (> 1 and < -1 kg km^{-2}
248 yr^{-1}) over North Africa, positive trends > 1 kg km^{-2} yr^{-1} parts of the Middle-East, and negative
249 trends < -1 kg km^{-2} yr^{-1} over northern China and southern Australia.
250
251 **4. Mean UVAI values for 2005-2015**
252 We examine the seasonal long-term mean UVAI values for insight into the spatial
253 distribution of the aerosol absorption signals. Figures 2 and 3 show the seasonal mean UVAI values
254 for 2005-2015 for OMI and the simulation, respectively. Positive UVAI values between 0.2 and
255 1.5 indicating aerosol absorption are present over major desert regions globally for both OMI and
256 the simulation, particularly over the Saharan, Iranian, and Thar deserts. These positive signals are
257 driven by the absorption by mineral dust (Herman et al., 1997; Torres et al., 1998; Buchard et al.,
258 2015). The simulation underestimates some of the smaller dust features captured by OMI, such as
259 over western North America, South America, Australia, and parts of Asia, perhaps reflecting an
260 underestimate in the simulated mineral dust lifetime (Ridley et al. 2012) and missing sources of
261 anthropogenic dust (Ginoux et al., 2012; Guan et al., 2016; Huang et al., 2015; Philip et al., 2017).
262 The seasonal variation in the observed and simulated UVAI is similar albeit with larger simulated
263 values in spring (MAM) over North Africa. In all seasons, the UVAI values driven by absorption
264 by dust in the simulation are concentrated mostly over North Africa, while for OMI the UVAI
265 values are more homogeneous over the Middle-East and Asia as well. Positive UVAI values of
266 ~0.2-1 over West and central Africa appearing in both the OMI and simulated values correspond
267 to absorption by brown carbon from biomass burning activities in these regions (Jethva and Torres,
268 2011; Hammer et al., 2016).
269
270
271
272 **5. Trend in UVAI values between 2005-2015**
273 Figure 4 shows the trend in OMI and simulated UVAI values (coincidently sampled from
274 OMI,) calculated from the GLS regression of monthly UVAI time series values over 2005-2015.
275 Cool colors indicate negative trend values, warm colors indicate positive trend values, and the
276 opacity of the colors indicates the statistical significance of the trends. Several regions exhibit
277 consistency between the OMI and simulated UVAI trends. Over the eastern United States there

are statistically significant, positive UVAI trends in OMI values of 1.0 $x10^{-5}$ to 2.5$x10^{-4}$ yr^{-1} and in simulated values of 2.5$x10^{-4}$ yr^{-1} to 5.0 $x10^{-4}$ yr^{-1}. Over Canada and parts of Russia there are statistically significant, positive UVAI trends in OMI values of 1.0 $x10^{-5}$ to 2.5$x10^{-4}$ yr^{-1} and in simulated values of 5.0 $x10^{-4}$ to 2.0$x10^{-3}$ yr^{-1}. Positive UVAI trends in both OMI and simulated values of 1.0 $x10^{-5}$ to 2.5$x10^{-4}$ yr^{-1} are present over Europe, although the simulated trends have low statistical significance. Statistically significant, positive UVAI trends in OMI values of 5.0 $x10^{-4}$ to 2.0 $x10^{-3}$ yr^{-1} are apparent over North Africa, which generally are captured by the simulation but with low statistical significance. Negative UVAI trends in both OMI and simulated values are present over West Africa, with low statistical significance that could be related to the filtering of persistent clouds. OMI and simulated UVAI values show negative trends of -2$x10^{-3}$ to -5.0$x10^{-4}$ yr^{-1} over India, although the simulated trends have lower statistical significance. Negative UVAI trends in both OMI and simulated values of -1.5$x10^{-3}$ yr^{-1} to -1.0$x10^{-5}$ yr^{-1} are apparent over most of South America, southern Africa, and Australia.

Some regions have trends in OMI UVAI values which are not captured by the simulation. Statistically significant, positive UVAI trends of 2.5$x10^{-4}$ yr^{-1} to 1.5 $x10^{-3}$ yr^{-1} over the western United States are apparent in the OMI values but not in the simulation. Zhang et al. (2017) found positive trends in aerosol absorption optical depth from OMI retrievals that they attributed to positive trends in mineral dust over the region, which were not captured by their GEOS-Chem simulation. Statistically significant, positive UVAI trends in OMI values between 5.0 $x10^{-4}$ to 2.0 $x10^{-3}$ yr^{-1} exist over the Middle-East, while the simulation has negative trends with low statistical significance. The OMI UVAI reveals a region of statistically significant, negative trends of -2$x10^{-3}$ to -5.0$x10^{-4}$ yr^{-1} over Mongolia/Inner Mongolia which is not captured by the simulation. There is also a small area of statistically significant, positive UVAI trends in OMI values of 1.5 $x10^{-3}$ to 2.0 $x10^{-3}$ yr^{-1} over Central Asia between the Caspian Sea and the Aral Sea which is not captured by the simulation. Trends in surface reflectance from the diminishing Aral Sea cannot solely explain the UVAI trends since they extend over the Caspian Sea. Trends in mineral dust are a more likely explanation as discussed further below.

Figures 5 and 6 show the seasonality of the OMI and simulated UVAI trends respectively. The positive UVAI trends over the eastern United States is strongest in summer (JJA) for both OMI and the simulation. The positive UVAI trends over North Africa and the Middle-East are present for all seasons for OMI and for most seasons in the simulation, except in JJA for North

Africa and spring (MAM) for the Middle-East. The negative trend in UVAI values over West Africa is most apparent in the fall (SON) and winter (DJF) for both OMI and the simulation. The negative OMI UVAI trends over Mongolia/Inner Mongolia and the positive OMI UVAI trends near the Aral Sea are strongest in JJA and weakest in DJF, providing evidence for a mineral dust source. Guan et al. (2017) examined dust storm data over northern China (including Inner Mongolia) for the period 1960-2007, and found that dust storm frequency has been declining over the region due to a gradual decrease in wind speed. The current generation of chemical transport models is unlikely to represent the source near the Aral Sea without an explicit parameterization of the drying sea. The desiccation of the Aral Sea over recent decades has resulted in a steady decline in water coverage over the area (Shi et al., 2014; Shi and Wang, 2015) and has led to the dried up sea bed becoming an increasing source of dust activity in the region (Spivak et al., 2012). Indoitu et al. (2015) found that most dust events are directed towards the west, consistent with the OMI observations. An increase in surface reflectance due to the drying up of the sea bed could also positively influence trends in UVAI. He et al. (2014) examined the 2000-2010 trends in global surface albedo using the Global Land Surface Satellites (GLASS) dataset and found a positive trend in surface albedo over the region in JJA and SON, corresponding to when the OMI UVAI trends are strongest.

6. Contribution of individual aerosol species to the simulated UVAI

To further interpret the UVAI trends, we examine the trends in aerosol concentrations from our GEOS-Chem simulation (Figure 7). Figure 7a shows the trends in secondary inorganic aerosol (SIA). There are statistically significant, negative trends over the eastern United States (-1 to -0.05 $\mu g\ m^{-2}\ yr^{-1}$) and statistically significant, positive trends over the Middle-East (0.05 to 0.5 $\mu g\ m^{-2}\ yr^{-1}$), India (0.05 to 1 $\mu g\ m^{-2}\ yr^{-1}$), South America, and southern Africa (0.05 to 0.25 $\mu g\ m^{-2}\ yr^{-1}$). Figure 7b shows the trends in dust. Similar to the trends in emissions, the trends in dust concentrations are of the largest magnitude of the various species, however often with low statistical significance. There are positive trends over the Middle-East (> 2 $\mu g\ m^{-2}\ yr^{-1}$), India (0.05 to 2 $\mu g\ m^{-2}\ yr^{-1}$), and north west China (1 to 2 $\mu g\ m^{-2}\ yr^{-1}$). There are also positive trends (0.05 to 0.25 $\mu g\ m^{-2}\ yr^{-1}$) with low statistical significance over the United States, northern South America, southern Africa, and northern Australia. There is a combination of positive and negative trends (> 2 and < -2 $\mu g\ m^{-2}\ yr^{-1}$) over North Africa, and negative trends over China and Mongolia (< -2 $\mu g\ m^{-2}\ yr^{-1}$) and Australia (-1 to -0.5 $\mu g\ m^{-2}\ yr^{-1}$). Figures 7c and 7d show the trends in total organic

aerosol (OA) and the absorbing brown carbon (BrC) component of OA, respectively. Positive trends over Canada and parts of Russia (0.05 to 0.5 μg m^{-2} yr^{-1}) in total OA are mainly due to the positive trend in BrC. Statistically significant, negative trends in total OA (-1 to -0.05 μg m^{-2} yr^{-1}) over the eastern United States are dominated by scattering organic aerosol. Statistically significant, negative trends (-2 to -0.05 μg m^{-2} yr^{-1}) over West Africa and South America for total OA are dominated by the trend in absorbing BrC. Figures 5e and 5f show the trends in black carbon (BC) and salt, respectively. There are positive trends (0.05 to 0.25 μg m^{-2} yr^{-1}) in BC with low statistical significance over India and China. Sea salt trends are negligible.

To gain further insight into how changes in aerosols effect the trends in simulated UVAI, we examine the sensitivity of the UVAI to changes in individual aerosol species. Figure 8 shows the change in annual mean UVAI due to doubling the concentration of individual aerosol species. Doubling scattering SIA concentrations (Figure 8a) decreases the UVAI between -0.25 and -0.1 over most of the globe, with the largest changes over the Eastern United States, Europe, parts of the Middle-East, India, and south east China. Doubling dust concentrations (Figure 8b) produces the largest changes in UVAI, causing increases between 0.5 and 1 over North Africa, and smaller increases between 0.2 and 0.5 over the Middle-East, Europe, and parts of Asia and Australia. Figures 8c and 8d show the changes in UVAI due to doubling total OA concentrations and the absorbing BrC component, respectively. The doubling of BrC increases the UVAI between 0.1 and 0.5 over Canada, West and central Africa, India, parts of Russia, eastern China, and central South America. Doubling total OA concentrations over central South America causes a net decrease of ~ -0.1 as the scattering component of total OA cancels out the absorption by BrC. Doubling BC concentrations (Figure 8e) increases the UVAI of 0.1 over central Africa, India, and south east China, while doubling sea salt concentrations (Figure 8f) has negligible effect on the UVAI.

Figure 9 shows the change in simulated UVAI due to the 2005-2015 trends in individual aerosol species from our GEOS-Chem simulation. The change for each species is calculated by applying the aerosol concentration trends for the individual aerosol type while leaving the concentrations unchanged for the other aerosol species, then taking the difference between this perturbed UVAI simulation and an unperturbed simulation. Negative trends in scattering SIA (Figure 9a) increase the UVAI by $1.0x10^{-4}$ to $7.5x10^{-3}$ yr^{-1} over the eastern United States and by $1.0x10^{-4}$ to $2.5x10^{-3}$ yr^{-1} over Europe, corresponding to regions of positive UVAI trends in both

OMI and the simulation (Figure 4). Increasing SIA decreases the UVAI by -2.5x10^{-3} yr^{-1} to -1.0x10^{-4} yr^{-1} over the Middle-East, India, and east China. Trends in dust concentrations (Figure 9b) cause the largest change in UVAI with regional increases > 1x10^{-2} yr^{-1} and regional decreases < -1x10^{-2} yr^{-1}. Simulated UVAI trends due to mineral dust are mostly negative over North Africa, East Asia, and Australia, while mostly positive over the Middle-East. Noisy trends in regional meteorology cause heterogeneous trends in dust and in the UVAI, with low statistical significance. Figures 9c and 9d show the change in UVAI due to the trends in total OA and the absorbing BrC component of total OA, respectively. Most of the changes in UVAI due to the trends in total OA are caused by the trends in the absorbing BrC component, with increases in the UVAI between 2.5x10^{-3} and 1x10^{-2} yr^{-1} over Canada and parts of Russia, corresponding to regions of positive UVAI trends for both OMI and the simulation (Figure 4). There are decreases in the UVAI < -1x10^{-2} yr^{-1} over central South America and West Africa due to the negative trends in BrC, corresponding to regions of negative UVAI trends for both OMI and the simulation (Figure 4). Over the eastern United States there is a mixture of increases and decreases in the UVAI due to the trends in scattering organic aerosol. Positive trends in BC increase the UVAI (Figure 9e) by 1.0x10^{-4} to 2.5x10^{-3} yr^{-1} over India and China. There are no obvious changes in the UVAI due to the trends in sea salt (Figure 9f).

7. Conclusions

Observations of aerosol scattering and absorption offer valuable information about aerosol composition. We simulated the Ultraviolet Aerosol Index (UVAI), a method of detecting aerosol absorption using satellite measurements, to interpret trends in OMI observed UVAI over 2005-2015 to understand global trends in aerosol composition. We conducted our simulation using the vector radiative transfer model VLIDORT with aerosol fields from the global chemical transport model GEOS-Chem.

We examined the 2005-2015 trends in individual aerosol species from GEOS-Chem, and applied these trends to the UVAI simulation to calculate the change in simulated UVAI due to the trends in individual aerosol species. We found that global trends in the UVAI were largely explained by trends in absorption by mineral dust, absorption by brown carbon, and scattering by secondary inorganic aerosols. The two most prominent positive trends in the observed UVAI were over North Africa and over Central Asia near the desiccating Aral Sea. The simulated UVAI

attributes the positive trends over North Africa to increasing mineral dust, despite an erroneous simulated negative trend in fall (SON) that deserves further attention. The positive trends in the observed UVAI over Central Asia near the shrinking Aral Sea are likely due to increased dust emissions, a feature that is unlikely to be represented in most chemical transport models. The most prominent negative trends in the observed UVAI were over East Asia, South Asia, and Australia. The simulation attributed the negative trends over East Asia and Australia to decreasing mineral dust, despite underestimating the trend in East Asia. The simulation attributed the negative trend over South Asia to increasing scattering secondary inorganic aerosols, a trend that the observations imply could be even larger. We found the positive trends in the UVAI over the eastern United States that were strongest in summer (JJA) in both the observations and the simulation were driven by a negative trend in scattering secondary inorganic aerosol (SIA). Observed negative trends in winter (DJF) were less well simulated. Over West Africa and South America, negative trends in UVAI were explained by negative trends in absorbing brown carbon.

Trends in the UVAI offer valuable information on the evolution of global aerosol composition that can be understood through quantitative simulation of the UVAI. The availability of the UVAI observations from 1979 to the present offer a unique opportunity to understand long-term trends in aerosol composition. The recent launch of TROPOMI and the forthcoming geostationary constellation offer UVAI observations at finer spatial and temporal resolution. The forthcoming MAIA satellite instrument offers an exciting opportunity to derive even more information about aerosol composition by combining measurements at ultraviolet wavelengths with multi-angle observations and polarization sensitivity.

Acknowledgements

This work was supported by the Natural Science and Engineering Research Council of Canada and the Killam Trusts. Computational facilities were provided in part by the Atlantic Computational Excellence Network and the Graham consortiums of Compute Canada.

References

Ahn, C., Torres, O. and Jethva, H.: Assessment of OMI near-UV aerosol optical depth over land, J. Geophys. Res. Atmos., 119(5), 2457–2473, doi:10.1002/2013JD020188, 2014.

Andela, N. and van der Werf, G. R.: Recent trends in African fires driven by cropland expansion and El Niño to La Niña transition, Nat. Clim. Chang., 4(9), 791–795, doi:10.1038/nclimate2313, 2014.

Andreae, M. O. and Gelencsér, A.: Black carbon or brown carbon? The nature of light-absorbing carbonaceous aerosols, Atmos. Chem. Phys., 6(10), 3131–3148, doi:10.5194/acp-6-3131-2006, 2006.

Badarinath, K. V. S., Kharol, S. K., Kaskaoutis, D. G., Sharma, A. R., Ramaswamy, V. and Kambezidis, H. D.: Long-range transport of dust aerosols over the Arabian Sea and Indian region — A case study using satellite data and ground-based measurements, Glob. Planet. Change, 72(3), 164–181, doi:10.1016/j.gloplacha.2010.02.003, 2010.

Bey, I., Jacob, D. J., Yantosca, R. M., Logan, J. A., Field, B. D., Fiore, A. M., Li, Q., Liu, H. Y., Mickley, L. J. and Schultz, M. G.: Global modeling of tropospheric chemistry with assimilated meteorology: Model description and evaluation, J. Geophys. Res., 106(D19), 23073, doi:10.1029/2001JD000807, 2001.

Bond, T. C., Doherty, S. J., Fahey, D. W., Forster, P. M., Berntsen, T., DeAngelo, B. J., Flanner, M. G., Ghan, S., Kärcher, B., Koch, D., Kinne, S., Kondo, Y., Quinn, P. K., Sarofim, M. C., Schultz, M. G., Schulz, M., Venkataraman, C., Zhang, H., Zhang, S., Bellouin, N., Guttikunda, S. K., Hopke, P. K., Jacobson, M. Z., Kaiser, J. W., Klimont, Z., Lohmann, U., Schwarz, J. P., Shindell, D., Storelvmo, T., Warren, S. G. and Zender, C. S.: Bounding the role of black carbon in the climate system: A scientific assessment, J. Geophys. Res. Atmos., 118(11), 5380–5552, doi:10.1002/jgrd.50171, 2013.

Boys, B. L., Martin, R. V., van Donkelaar, A., MacDonell, R. J., Hsu, N. C., Cooper, M. J., Yantosca, R. M., Lu, Z., Streets, D. G., Zhang, Q. and Wang, S. W.: Fifteen-Year Global Time Series of Satellite-Derived Fine Particulate Matter, Environ. Sci. Technol., 48(19), 11109–11118, doi:10.1021/es502113p, 2014.

Buchard, V., da Silva, A. M., Colarco, P. R., Darmenov, A., Randles, C. A., Govindaraju, R., Torres, O., Campbell, J. and Spurr, R.: Using the OMI aerosol index and absorption aerosol optical depth to evaluate the NASA MERRA Aerosol Reanalysis, Atmos. Chem. Phys., 15(10), 5743–5760, doi:10.5194/acp-15-5743-2015, 2015.

Chen, Y., Morton, D. C., Jin, Y., Collatz, G. J., Kasibhatla, P. S., van der Werf, G. R., DeFries, R. S. and Randerson, J. T.: Long-term trends and interannual variability of forest, savanna and agricultural fires in South America, Carbon Manag., 4(6), 617–638, doi:10.4155/cmt.13.61, 2013.

Chin, M., Diehl, T., Tan, Q., Prospero, J. M., Kahn, R. A., Remer, L. A., Yu, H., Sayer, A. M., Bian, H., Geogdzhayev, I. V., Holben, B. N., Howell, S. G., Huebert, B. J., Hsu, N. C., Kim, D., Kucsera, T. L., Levy, R. C., Mishchenko, M. I., Pan, X., Quinn, P. K., Schuster, G. L., Streets, D. G., Strode, S. A., Torres, O. and Zhao, X.-P.: Multi-decadal aerosol variations from 1980 to 2009: a perspective from observations and a global model, Atmos. Chem. Phys., 14(7), 3657–3690, doi:10.5194/acp-14-3657-2014, 2014a.

475 Chin, M., Diehl, T., Tan, Q., Prospero, J. M., Kahn, R. A., Remer, L. A., Yu, H., Sayer, A. M.,
476 Bian, H., Geogdzhayev, I. V., Holben, B. N., Howell, S. G., Huebert, B. J., Hsu, N. C., Kim, D.,
477 Kucsera, T. L., Levy, R. C., Mishchenko, M. I., Pan, X., Quinn, P. K., Schuster, G. L., Streets,
478 D. G., Strode, S. A., Torres, O. and Zhao, X.-P.: Multi-decadal aerosol variations from 1980 to
479 2009: a perspective from observations and a global model, Atmos. Chem. Phys., 14(7), 3657–
480 3690, doi:10.5194/acp-14-3657-2014, 2014b.

481 Crippa, M., Janssens-Maenhout, G., Dentener, F., Guizzardi, D., Sindelarova, K., Muntean, M.,
482 Van Dingenen, R. and Granier, C.: Forty years of improvements in European air quality: regional
483 policy-industry interactions with global impacts, Atmos. Chem. Phys., 16(6), 3825–3841,
484 doi:10.5194/acp-16-3825-2016, 2016.

485 Cui, H., Mao, P., Zhao, Y., Nielsen, C. P. and Zhang, J.: Patterns in atmospheric carbonaceous
486 aerosols in China: emission estimates and observed concentrations, Atmos. Chem. Phys., 15(15),
487 8657–8678, doi:10.5194/acp-15-8657-2015, 2015.

488 Curci, G., Hogrefe, C., Bianconi, R., Im, U., Balzarini, A., Baró, R., Brunner, D., Forkel, R.,
489 Giordano, L., Hirtl, M., Honzak, L., Jiménez-Guerrero, P., Knote, C., Langer, M., Makar, P. A.,
490 Pirovano, G., Pérez, J. L., San José, R., Syrakov, D., Tuccella, P., Werhahn, J., Wolke, R.,
491 Žabkar, R., Zhang, J. and Galmarini, S.: Uncertainties of simulated aerosol optical properties
492 induced by assumptions on aerosol physical and chemical properties: An AQMEII-2 perspective,
493 Atmos. Environ., 115, 541–552, doi:10.1016/j.atmosenv.2014.09.009, 2015.

494 Curier, L., Kranenburg, R., Timmermans, R., Segers, A., Eskes, H. and Schaap, M.: Synergistic
495 Use of LOTOS-EUROS and NO2 Tropospheric Columns to Evaluate the NOX Emission Trends
496 Over Europe, pp. 239–245., 2014.

497 Deirmendjian, D.: Scattering and Polarization Properties of Water Clouds and Hazes in the
498 Visible and Infrared, Appl. Opt., 3(2), 187, doi:10.1364/AO.3.000187, 1964.

499 Dey, S. and Di Girolamo, L.: A decade of change in aerosol properties over the Indian
500 subcontinent, Geophys. Res. Lett., 38(14), n/a-n/a, doi:10.1029/2011GL048153, 2011.

501 Drury, E., Jacob, D. J., Spurr, R. J. D., Wang, J., Shinozuka, Y., Anderson, B. E., Clarke, A. D.,
502 Dibb, J., McNaughton, C. and Weber, R.: Synthesis of satellite (MODIS), aircraft (ICARTT),
503 and surface (IMPROVE, EPA-AQS, AERONET) aerosol observations over eastern North
504 America to improve MODIS aerosol retrievals and constrain surface aerosol concentrations and
505 sources, J. Geophys. Res., 115(D14), D14204, doi:10.1029/2009JD012629, 2010.

506 Duncan, B. N., Martin, R. V., Staudt, A. C., Yevich, R. and Logan, J. A.: Interannual and
507 seasonal variability of biomass burning emissions constrained by satellite observations, J.
508 Geophys. Res., 108(D2), 4100, doi:10.1029/2002JD002378, 2003.

509 Fairlie, D. J., Jacob, D. J. and Park, R. J.: The impact of transpacific transport of mineral dust in
510 the United States, Atmos. Environ., 41(6), 1251–1266, doi:10.1016/j.atmosenv.2006.09.048,
511 2007.

512 Fountoukis, C. and Nenes, A.: ISORROPIA II: a computationally efficient thermodynamic
513 equilibrium model for K^+–Ca^{2+}–Mg^{2+}–NH_4^+–Na^+–SO_4^{2-}–NO_3^-–Cl^-–H_2O aero, Atmos. Chem.
514 Phys., 7(17), 4639–4659, doi:10.5194/acp-7-4639-2007, 2007.

515 Giglio, L., Randerson, J. T. and van der Werf, G. R.: Analysis of daily, monthly, and annual
516 burned area using the fourth-generation global fire emissions database (GFED4), J. Geophys.

517 Res. Biogeosciences, 118(1), 317–328, doi:10.1002/jgrg.20042, 2013.

518 Ginoux, P., Prospero, J. M., Gill, T. E., Hsu, N. C. and Zhao, M.: Global-scale attribution of
519 anthropogenic and natural dust sources and their emission rates based on MODIS Deep Blue
520 aerosol products, Rev. Geophys., 50(3), doi:10.1029/2012RG000388, 2012.

521 de Graaf, M., Stammes, P., Torres, O. and Koelemeijer, R. B. A.: Absorbing Aerosol Index:
522 Sensitivity analysis, application to GOME and comparison with TOMS, J. Geophys. Res.,
523 110(D1), D01201, doi:10.1029/2004JD005178, 2005.

524 Guan, H., Esswein, R., Lopez, J., Bergstrom, R., Warnock, A., Follette-Cook, M., Fromm, M.
525 and Iraci, L. T.: A multi-decadal history of biomass burning plume heights identified using
526 aerosol index measurements, Atmos. Chem. Phys., 10(14), 6461–6469, doi:10.5194/acp-10-
527 6461-2010, 2010.

528 Guan, Q., Sun, X., Yang, J., Pan, B., Zhao, S., Wang, L., Guan, Q., Sun, X., Yang, J., Pan, B.,
529 Zhao, S. and Wang, L.: Dust Storms in Northern China: Long-Term Spatiotemporal
530 Characteristics and Climate Controls, J. Clim., 30(17), 6683–6700, doi:10.1175/JCLI-D-16-
531 0795.1, 2017.

532 Guan, X., Huang, J., Zhang, Y., Xie, Y. and Liu, J.: The relationship between anthropogenic dust
533 and population over global semi-arid regions, Atmos. Chem. Phys., 16(8), 5159–5169,
534 doi:10.5194/acp-16-5159-2016, 2016.

535 Guo, Y., Tian, B., Kahn, R. A., Kalashnikova, O., Wong, S. and Waliser, D. E.: Tropical Atlantic
536 dust and smoke aerosol variations related to the Madden-Julian Oscillation in MODIS and MISR
537 observations, J. Geophys. Res. Atmos., 118(10), 4947–4963, doi:10.1002/jgrd.50409, 2013.

538 Hammer, M. S., Martin, R. V., van Donkelaar, A., Buchard, V., Torres, O., Ridley, D. A. and
539 Spurr, R. J. D.: Interpreting the ultraviolet aerosol index observed with the OMI satellite
540 instrument to understand absorption by organic aerosols: implications for atmospheric oxidation
541 and direct radiative effects, Atmos. Chem. Phys., 16(4), 2507–2523, doi:10.5194/acp-16-2507-
542 2016, 2016.

543 He, T., Liang, S. and Song, D.-X.: Analysis of global land surface albedo climatology and
544 spatial-temporal variation during 1981-2010 from multiple satellite products, J. Geophys. Res.
545 Atmos., 119(17), 10,281-10,298, doi:10.1002/2014JD021667, 2014.

546 Heald, C. L., J. L. Collett Jr., J. L., Lee, T., Benedict, K. B., Schwandner, F. M., Li, Y., Clarisse,
547 L., Hurtmans, D. R., Van Damme, M., Clerbaux, C., Coheur, P.-F., Philip, S., Martin, R. V. and
548 Pye, H. O. T.: Atmospheric ammonia and particulate inorganic nitrogen over the United States,
549 Atmos. Chem. Phys., 12(21), 10295–10312, doi:10.5194/acp-12-10295-2012, 2012.

550 Herman, J. R., Bhartia, P. K., Torres, O., Hsu, C., Seftor, C. and Celarier, E.: Global distribution
551 of UV-absorbing aerosols from Nimbus 7/TOMS data, J. Geophys. Res., 102(D14), 16911,
552 doi:10.1029/96JD03680, 1997.

553 Hsu, N. C., Gautam, R., Sayer, A. M., Bettenhausen, C., Li, C., Jeong, M. J., Tsay, S.-C. and
554 Holben, B. N.: Global and regional trends of aerosol optical depth over land and ocean using
555 SeaWiFS measurements from 1997 to 2010, Atmos. Chem. Phys. Atmos. Chem. Phys., 12,
556 8037–8053, doi:10.5194/acp-12-8037-2012, 2012.

557 Huang, J., Minnis, P., Yan, H., Yi, Y., Chen, B., Zhang, L. and Ayers, J. K.: Dust aerosol effect

558 on semi-arid climate over Northwest China detected from A-Train satellite measurements,
559 Atmos. Chem. Phys., 10(14), 6863–6872, doi:10.5194/acp-10-6863-2010, 2010.

560 Huang, J. P., Liu, J. J., Chen, B. and Nasiri, S. L.: Detection of anthropogenic dust using
561 CALIPSO lidar measurements, Atmos. Chem. Phys., 15(20), 11653–11665, doi:10.5194/acp-15-
562 11653-2015, 2015.

563 Indoitu, R., Kozhoridze, G., Batyrbaeva, M., Vitkovskaya, I., Orlovsky, N., Blumberg, D. and
564 Orlovsky, L.: Dust emission and environmental changes in the dried bottom of the Aral Sea,
565 Aeolian Res., 17, 101–115, doi:10.1016/j.aeolia.2015.02.004, 2015.

566 IPCC: Climate Change 2014: Impacts, Adaptation, and Vulnerability. Part A: Global and
567 Sectoral Aspects. Contribution of Working Group II to the Fifth Assessment Report of the
568 Intergovernmental Panel on Climate Change [Field, C.B., V.R. Barros, D.J. Dokken, K.J.,
569 Cambridge University Press, Cambridge, United Kingdom and New York, NY, USA., 2014.

570 Israelevich, P. L., Levin, Z., Joseph, J. H. and Ganor, E.: Desert aerosol transport in the
571 Mediterranean region as inferred from the TOMS aerosol index, J. Geophys. Res. Atmos.,
572 107(D21), AAC 13-1-AAC 13-13, doi:10.1029/2001JD002011, 2002.

573 Jaeglé, L., Quinn, P. K., Bates, T. S., Alexander, B. and Lin, J.-T.: Global distribution of sea salt
574 aerosols: new constraints from in situ and remote sensing observations, Atmos. Chem. Phys.,
575 11(7), 3137–3157, doi:10.5194/acp-11-3137-2011, 2011.

576 Jethva, H. and Torres, O.: Satellite-based evidence of wavelength-dependent aerosol absorption
577 in biomass burning smoke inferred from Ozone Monitoring Instrument, Atmos. Chem. Phys.,
578 11(20), 10541–10551, doi:10.5194/acp-11-10541-2011, 2011.

579 Jethva, H., Torres, O. and Ahn, C.: Global assessment of OMI aerosol single-scattering albedo
580 using ground-based AERONET inversion, J. Geophys. Res. Atmos., 119(14), 9020–9040,
581 doi:10.1002/2014JD021672, 2014.

582 Kahn, R. A. and Gaitley, B. J.: An analysis of global aerosol type as retrieved by MISR, J.
583 Geophys. Res. Atmos., 120(9), 4248–4281, doi:10.1002/2015JD023322, 2015.

584 Kalashnikova, O. V. and Kahn, R. A.: Mineral dust plume evolution over the Atlantic from
585 MISR and MODIS aerosol retrievals, J. Geophys. Res., 113(D24), D24204,
586 doi:10.1029/2008JD010083, 2008.

587 Kaskaoutis, D. G., Kharol, S. K., Sifakis, N., Nastos, P. T., Sharma, A. R., Badarinath, K. V. S.
588 and Kambezidis, H. D.: Satellite monitoring of the biomass-burning aerosols during the wildfires
589 of August 2007 in Greece: Climate implications, Atmos. Environ., 45(3), 716–726,
590 doi:10.1016/j.atmosenv.2010.09.043, 2011.

591 Klimont, Z., Smith, S. J. and Cofala, J.: The last decade of global anthropogenic sulfur dioxide:
592 2000–2011 emissions, Environ. Res. Lett. Environ. Res. Lett, 8(8), 14003–6, doi:10.1088/1748-
593 9326/8/1/014003, 2013.

594 Klimont, Z., Kupiainen, K., Heyes, C., Purohit, P., Cofala, J., Rafaj, P., Borken-Kleefeld, J. and
595 Schöpp, W.: Global anthropogenic emissions of particulate matter including black carbon,
596 Atmos. Chem. Phys., 17(14), 8681–8723, doi:10.5194/acp-17-8681-2017, 2017.

597 Koepke, P., Hess, M., Schult, I. and Shettle, E. P.: Global Aerosol Dataset, report, Max-Planck
598 Inst. fur Meteorol., Hamburg, Germany., 1997.

599 Kristiansen, N. I., Stohl, A., Olivié, D. J. L., Croft, B., Søvde, O. A., Klein, H., Christoudias, T.,
600 Kunkel, D., Leadbetter, S. J., Lee, Y. H., Zhang, K., Tsigaridis, K., Bergman, T., Evangeliou, N.,
601 Wang, H., Ma, P.-L., Easter, R. C., Rasch, P. J., Liu, X., Pitari, G., Di Genova, G., Zhao, S. Y.,
602 Balkanski, Y., Bauer, S. E., Faluvegi, G. S., Kokkola, H., Martin, R. V., Pierce, J. R., Schulz, M.,
603 Shindell, D., Tost, H. and Zhang, H.: Evaluation of observed and modelled aerosol lifetimes
604 using radioactive tracers of opportunity and an ensemble of 19 global models, Atmos. Chem.
605 Phys., 16(5), 3525–3561, doi:10.5194/acp-16-3525-2016, 2016.

606 Kuhns, H., Knipping, E. M. and Vukovich, J. M.: Development of a United States–Mexico
607 Emissions Inventory for the Big Bend Regional Aerosol and Visibility Observational (BRAVO)
608 Study, J. Air Waste Manage. Assoc., 55(5), 677–692, doi:10.1080/10473289.2005.10464648,
609 2005.

610 Lee, C., Martin, R. V., van Donkelaar, A., O'Byrne, G., Krotkov, N., Richter, A., Huey, L. G.
611 and Holloway, J. S.: Retrieval of vertical columns of sulfur dioxide from SCIAMACHY and
612 OMI: Air mass factor algorithm development, validation, and error analysis, J. Geophys. Res.,
613 114(D22), D22303, doi:10.1029/2009JD012123, 2009.

614 Leibensperger, E. M., Mickley, L. J., Jacob, D. J., Chen, W.-T., Seinfeld, J. H., Nenes, A.,
615 Adams, P. J., Streets, D. G., Kumar, N. and Rind, D.: Climatic effects of 1950–2050 changes in
616 US anthropogenic aerosols – Part 2: Climate response, Atmos. Chem. Phys., 12(7), 3349–3362,
617 doi:10.5194/acp-12-3349-2012, 2012.

618 Li, C., Martin, R. V., van Donkelaar, A., Boys, B. L., Hammer, M. S., Xu, J.-W., Marais, E. A.,
619 Reff, A., Strum, M., Ridley, D. A., Crippa, M., Brauer, M. and Zhang, Q.: Trends in Chemical
620 Composition of Global and Regional Population-Weighted Fine Particulate Matter Estimated for
621 25 Years, Environ. Sci. Technol., acs.est.7b02530, doi:10.1021/acs.est.7b02530, 2017a.

622 Li, M., Zhang, Q., Kurokawa, J., Woo, J.-H., He, K., Lu, Z., Ohara, T., Song, Y., Streets, D. G.,
623 Carmichael, G. R., Cheng, Y., Hong, C., Huo, H., Jiang, X., Kang, S., Liu, F., Su, H. and Zheng,
624 B.: MIX: a mosaic Asian anthropogenic emission inventory under the international collaboration
625 framework of the MICS-Asia and HTAP, Atmos. Chem. Phys., 17(2), 935–963,
626 doi:10.5194/acp-17-935-2017, 2017b.

627 Liu, F., Zhang, Q., van der A, R. J., Zheng, B., Tong, D., Yan, L., Zheng, Y. and He, K.: Recent
628 reduction in NO $_x$ emissions over China: synthesis of satellite observations and emission
629 inventories, Environ. Res. Lett., 11(11), 114002, doi:10.1088/1748-9326/11/11/114002, 2016.

630 Liu, Y., Koutrakis, P. and Kahn, R.: Estimating fine particulate matter component concentrations
631 and size distributions using satellite-retrieved fractional aerosol optical depth: part 1--method
632 development., J. Air Waste Manag. Assoc., 57(11), 1351–9 [online] Available from:
633 http://www.ncbi.nlm.nih.gov/pubmed/18069458 (Accessed 6 September 2017), 2007.

634 Lu, Z., Zhang, Q. and Streets, D. G.: Sulfur dioxide and primary carbonaceous aerosol emissions
635 in China and India, Atmos. Chem. Phys. Atmos. Chem. Phys., 11, 9839–9864, doi:10.5194/acp-
636 11-9839-2011, 2011.

637 Mann, M. E. and Emanuel, K. A.: Atlantic hurricane trends linked to climate change, Eos, Trans.
638 Am. Geophys. Union, 87(24), 233, doi:10.1029/2006EO240001, 2006.

639 Mao, K. B., Ma, Y., Xia, L., Chen, W. Y., Shen, X. Y., He, T. J. and Xu, T. R.: Global aerosol
640 change in the last decade: An analysis based on MODIS data, Atmos. Environ., 94, 680–686,

641 doi:10.1016/j.atmosenv.2014.04.053, 2014.

642 Marais, E. A., Jacob, D. J., Jimenez, J. L., Campuzano-Jost, P., Day, D. A., Hu, W., Krechmer,
643 J., Zhu, L., Kim, P. S., Miller, C. C., Fisher, J. A., Travis, K., Yu, K., Hanisco, T. F., Wolfe, G.
644 M., Arkinson, H. L., Pye, H. O. T., Froyd, K. D., Liao, J. and McNeill, V. F.: Aqueous-phase
645 mechanism for secondary organic aerosol formation from isoprene: application to the southeast
646 United States and co-benefit of SO₂ emission controls, Atmos. Chem.
647 Phys., 16(3), 1603–1618, doi:10.5194/acp-16-1603-2016, 2016.

648 Martin, R. V., Jacob, D. J., Yantosca, R. M., Chin, M. and Ginoux, P.: Global and regional
649 decreases in tropospheric oxidants from photochemical effects of aerosols, J. Geophys. Res.,
650 108(D3), 4097, doi:10.1029/2002JD002622, 2003.

651 Mauritsen, T.: Arctic climate change: Greenhouse warming unleashed, Nat. Geosci., 9(4), 271–
652 272, doi:10.1038/ngeo2677, 2016.

653 Mehta, M., Singh, R., Singh, A., Singh, N. and Anshumali: Recent global aerosol optical depth
654 variations and trends — A comparative study using MODIS and MISR level 3 datasets, Remote
655 Sens. Environ., 181, 137–150, doi:10.1016/j.rse.2016.04.004, 2016.

656 de Meij, A., Pozzer, A. and Lelieveld, J.: Trend analysis in aerosol optical depths and pollutant
657 emission estimates between 2000 and 2009, Atmos. Environ., 51, 75–85,
658 doi:10.1016/j.atmosenv.2012.01.059, 2012.

659 Mielonen, T., Portin, H., Komppula, M., Leskinen, A., Tamminen, J., Ialongo, I., Hakkarainen,
660 J., Lehtinen, K. E. J. and Arola, A.: Biomass burning aerosols observed in Eastern Finland
661 during the Russian wildfires in summer 2010 – Part 2: Remote sensing, Atmos. Environ., 47,
662 279–287, doi:10.1016/j.atmosenv.2011.07.016, 2012.

663 Moosmüller, H., Chakrabarty, R. K. and Arnott, W. P.: Aerosol light absorption and its
664 measurement: A review, J. Quant. Spectrosc. Radiat. Transf., 110(11), 844–878,
665 doi:10.1016/j.jqsrt.2009.02.035, 2009.

666 Park, R. J., Jacob, D. J., Chin, M. and Martin, R. V.: Sources of carbonaceous aerosols over the
667 United States and implications for natural visibility, J. Geophys. Res., 108(D12), 4355,
668 doi:10.1029/2002JD003190, 2003.

669 Park, R. J., Jacob, D. J., Field, B. D., Yantosca, R. M. and Chin, M.: Natural and transboundary
670 pollution influences on sulfate-nitrate-ammonium aerosols in the United States: Implications for
671 policy, J. Geophys. Res., 109(D15), D15204, doi:10.1029/2003JD004473, 2004.

672 Philip, S., Martin, R. V, Snider, G., Weagle, C. L., van Donkelaar, A., Brauer, M., Henze, D. K.,
673 Klimont, Z., Venkataraman, C., Guttikunda, S. K. and Zhang, Q.: Anthropogenic fugitive,
674 combustion and industrial dust is a significant, underrepresented fine particulate matter source in
675 global atmospheric models, Environ. Res. Lett., 12(4), 44018, doi:10.1088/1748-9326/aa65a4,
676 2017.

677 Pöschl, U.: Atmospheric Aerosols: Composition, Transformation, Climate and Health Effects,
678 Angew. Chemie Int. Ed., 44(46), 7520–7540, doi:10.1002/anie.200501122, 2005.

679 Pye, H. O. T., Liao, H., Wu, S., Mickley, L. J., Jacob, D. J., Henze, D. K. and Seinfeld, J. H.:
680 Effect of changes in climate and emissions on future sulfate-nitrate-ammonium aerosol levels in
681 the United States, J. Geophys. Res., 114(D1), D01205, doi:10.1029/2008JD010701, 2009.

682 Pye, H. O. T., Chan, A. W. H., Barkley, M. P. and Seinfeld, J. H.: Global modeling of organic
683 aerosol: the importance of reactive nitrogen (NO_x and
684 NO₃), Atmos. Chem. Phys., 10(22), 11261–11276, doi:10.5194/acp-10-
685 11261-2010, 2010.

686 Ramanathan, V. and Carmichael, G.: Global and regional climate changes due to black carbon,
687 Nat. Geosci., 1(4), 221–227, doi:10.1038/ngeo156, 2008.

688 Ridley, D. A., Heald, C. L. and Ford, B.: North African dust export and deposition: A satellite
689 and model perspective, J. Geophys. Res., 117(D2), D02202, doi:10.1029/2011JD016794, 2012.

690 Schepanski, K., Tegen, I., Laurent, B., Heinold, B. and Macke, A.: A new Saharan dust source
691 activation frequency map derived from MSG-SEVIRI IR-channels, Geophys. Res. Lett., 34(18),
692 L18803, doi:10.1029/2007GL030168, 2007.

693 Scollo, S., Kahn, R. A., Nelson, D. L., Coltelli, M., Diner, D. J., Garay, M. J. and Realmuto, V.
694 J.: MISR observations of Etna volcanic plumes, J. Geophys. Res. Atmos., 117(D6), n/a-n/a,
695 doi:10.1029/2011JD016625, 2012.

696 Shao, Y., Klose, M. and Wyrwoll, K.-H.: Recent global dust trend and connections to climate
697 forcing, J. Geophys. Res. Atmos., 118(19), 11,107-11,118, doi:10.1002/jgrd.50836, 2013.

698 Shi, W. and Wang, M.: Decadal changes of water properties in the Aral Sea observed by
699 MODIS-Aqua, J. Geophys. Res. Ocean., 120(7), 4687–4708, doi:10.1002/2015JC010937, 2015.

700 Shi, W., Wang, M. and Guo, W.: Long-term hydrological changes of the Aral Sea observed by
701 satellites, J. Geophys. Res. Ocean., 119(6), 3313–3326, doi:10.1002/2014JC009988, 2014.

702 Simon, H., Reff, A., Wells, B., Xing, J. and Frank, N.: Ozone Trends Across the United States
703 over a Period of Decreasing NOx and VOC Emissions, 2014.

704 Spivak, L., Terechov, A., Vitkovskaya, I., Batyrbayeva, M. and Orlovsky, L.: Dynamics of Dust
705 Transfer from the Desiccated Aral Sea Bottom Analysed by Remote Sensing, pp. 97–106,
706 Springer, Berlin, Heidelberg., 2012.

707 Spurr, R. J. D.: VLIDORT: A linearized pseudo-spherical vector discrete ordinate radiative
708 transfer code for forward model and retrieval studies in multilayer multiple scattering media, J.
709 Quant. Spectrosc. Radiat. Transf., 102(2), 316–342, doi:10.1016/j.jqsrt.2006.05.005, 2006.

710 Stier, P., Seinfeld, J. H., Kinne, S. and Boucher, O.: Aerosol absorption and radiative forcing,
711 Atmos. Chem. Phys., 7(19), 5237–5261, doi:10.5194/acp-7-5237-2007, 2007.

712 Storelvmo, T., Leirvik, T., Lohmann, U., Phillips, P. C. B. and Wild, M.: Disentangling
713 greenhouse warming and aerosol cooling to reveal Earth's climate sensitivity, Nat. Geosci., 9(4),
714 286–289, doi:10.1038/ngeo2670, 2016.

715 Torres, O., Bhartia, P. K., Herman, J. R., Ahmad, Z. and Gleason, J.: Derivation of aerosol
716 properties from satellite measurements of backscattered ultraviolet radiation: Theoretical basis, J.
717 Geophys. Res., 103(D14), 17099, doi:10.1029/98JD00900, 1998.

718 Torres, O., Tanskanen, A., Veihelmann, B., Ahn, C., Braak, R., Bhartia, P. K., Veefkind, P. and
719 Levelt, P.: Aerosols and surface UV products from Ozone Monitoring Instrument observations:
720 An overview, J. Geophys. Res., 112(D24), D24S47, doi:10.1029/2007JD008809, 2007.

721 Torres, O., Chen, Z., Jethva, H., Ahn, C., Freitas, S. R. and Bhartia, P. K.: OMI and MODIS

722 observations of the anomalous 2008–2009 Southern Hemisphere biomass burning seasons,
723 Atmos. Chem. Phys., 10(8), 3505–3513, doi:10.5194/acp-10-3505-2010, 2010.

724 Torres, O., Ahn, C. and Chen, Z.: Improvements to the OMI near-UV aerosol algorithm using A-
725 train CALIOP and AIRS observations, Atmos. Meas. Tech., 6(11), 3257–3270, doi:10.5194/amt-
726 6-3257-2013, 2013.

727 Travis, K. R., Jacob, D. J., Fisher, J. A., Kim, P. S., Marais, E. A., Zhu, L., Yu, K., Miller, C. C.,
728 Yantosca, R. M., Sulprizio, M. P., Thompson, A. M., Wennberg, P. O., Crounse, J. D., St. Clair,
729 J. M., Cohen, R. C., Laughner, J. L., Dibb, J. E., Hall, S. R., Ullmann, K., Wolfe, G. M., Pollack,
730 I. B., Peischl, J., Neuman, J. A. and Zhou, X.: Why do models overestimate surface ozone in the
731 Southeast United States?, Atmos. Chem. Phys., 16(21), 13561–13577, doi:10.5194/acp-16-
732 13561-2016, 2016.

733 Wang, S., Zhang, Q., Martin, R. V, Philip, S., Liu, F., Li, M., Jiang, X. and He, K.: Satellite
734 measurements oversee China's sulfur dioxide emission reductions from coal-fired power plants,
735 Environ. Res. Lett., 10(11), 114015, doi:10.1088/1748-9326/10/11/114015, 2015.

736 Xing, J., Mathur, R., Pleim, J., Hogrefe, C., Gan, C.-M., Wong, D. C., Wei, C., Gilliam, R. and
737 Pouliot, G.: Observations and modeling of air quality trends over 1990–2010 across the Northern
738 Hemisphere: China, the United States and Europe, Atmos. Chem. Phys., 15(5), 2723–2747,
739 doi:10.5194/acp-15-2723-2015, 2015.

740 Zhang, L., Henze, D. K., Grell, G. A., Torres, O., Jethva, H. and Lamsal, L. N.: What factors
741 control the trend of increasing AAOD over the United States in the last decade?, J. Geophys.
742 Res. Atmos., 122(3), 1797–1810, doi:10.1002/2016JD025472, 2017.

743 Zhang, W., Gu, X., Xu, H., Yu, T. and Zheng, F.: Assessment of OMI near-UV aerosol optical
744 depth over Central and East Asia, J. Geophys. Res. Atmos., 121(1), 382–398,
745 doi:10.1002/2015JD024103, 2016.

746 Zhao, B., Wang, S. X., Liu, H., Xu, J. Y., Fu, K., Klimont, Z., Hao, J. M., He, K. B., Cofala, J.
747 and Amann, M.: NO x emissions in China: historical trends and future perspectives, Atmos.
748 Chem. Phys, 13, 9869–9897, doi:10.5194/acp-13-9869-2013, 2013.

749
750
751
752
753
754
755
756
757
758
759

Atmos. Chem. Phys. Discuss., https://doi.org/10.5194/acp-2017-1183
Manuscript under review for journal Atmos. Chem. Phys.
Discussion started: 12 February 2018

Atmospheric Chemistry and Physics Discussions

760 **Figures**

761

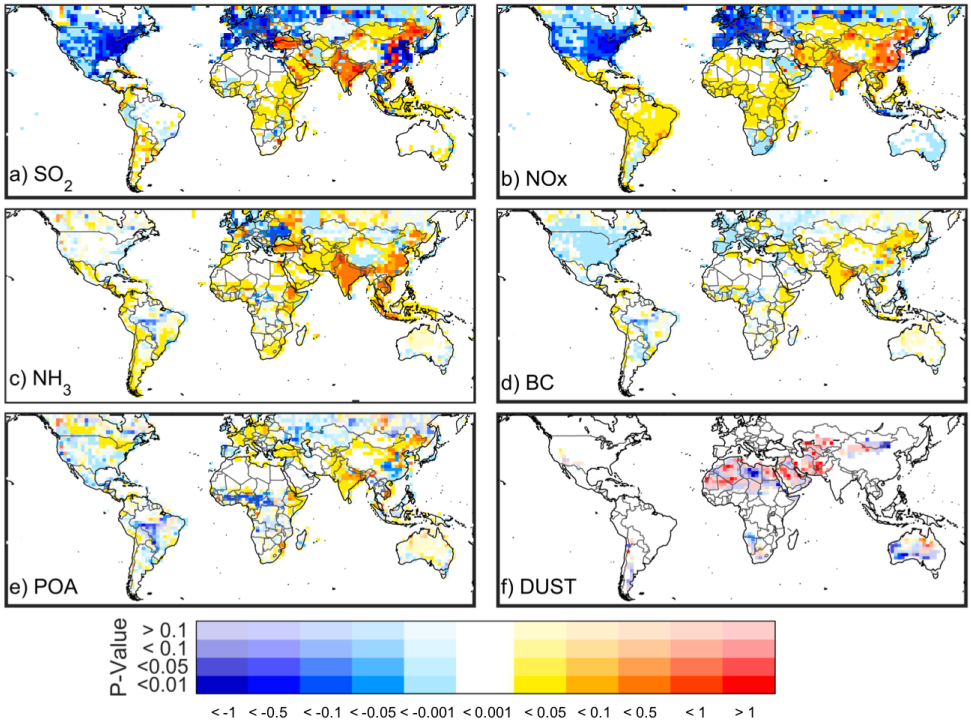

762

763 **Figure 1:** Trend in emissions of a) sulfur dioxide (SO_2) (kg SO_2 km^{-2} yr^{-1}), b) nitrogen oxides
764 (NO_x) (kg NO km^{-2} yr^{-1}), ammonia (NH_3) (kg NH_3 km^{-2} yr^{-1}), black carbon (BC) (kg C km^{-2} yr^{-1}),
765 primary organic carbon (POA) (kg C km^{-2} yr^{-1}), and dust (kg km^{-2} yr^{-1}) used in our GEOS-Chem
766 simulation. The trends are calculated from the Generalized Least Squares regression of monthly
767 time series values over 2005-2015.

768

Atmos. Chem. Phys. Discuss., https://doi.org/10.5194/acp-2017-1183
Manuscript under review for journal Atmos. Chem. Phys.
Discussion started: 12 February 2018

Atmospheric Chemistry and Physics Discussions

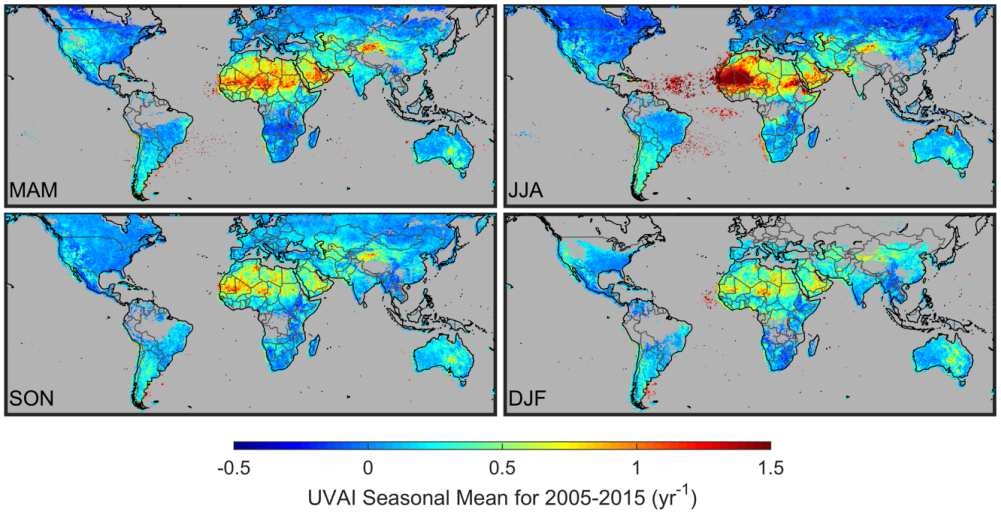

Figure 2: Seasonal mean UVAI values for the 2005-2015 period as observed by OMI for MAM (May, April, March), JJA (June, July August), SON (September, October, November), and DJF (December, January, February). Gray indicates persistent cloud fraction greater than 5%.

Atmos. Chem. Phys. Discuss., https://doi.org/10.5194/acp-2017-1183
Manuscript under review for journal Atmos. Chem. Phys.
Discussion started: 12 February 2018

Atmospheric Chemistry and Physics Discussions

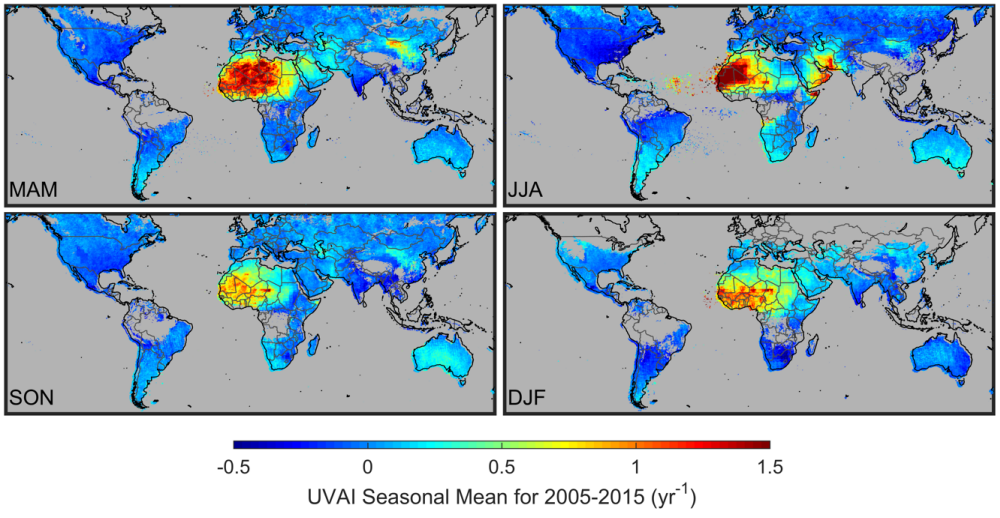

782

783 **Figure 3:** Seasonal mean UVAI values for the 2005-2015 period from our simulation coincidently
784 sampled from OMI for MAM (May, April, March), JJA (June, July August), SON (September,
785 October, November), and DJF (December, January, February). Gray indicates persistent cloud
786 fraction greater than 5%.

Atmos. Chem. Phys. Discuss., https://doi.org/10.5194/acp-2017-1183
Manuscript under review for journal Atmos. Chem. Phys.
Discussion started: 12 February 2018

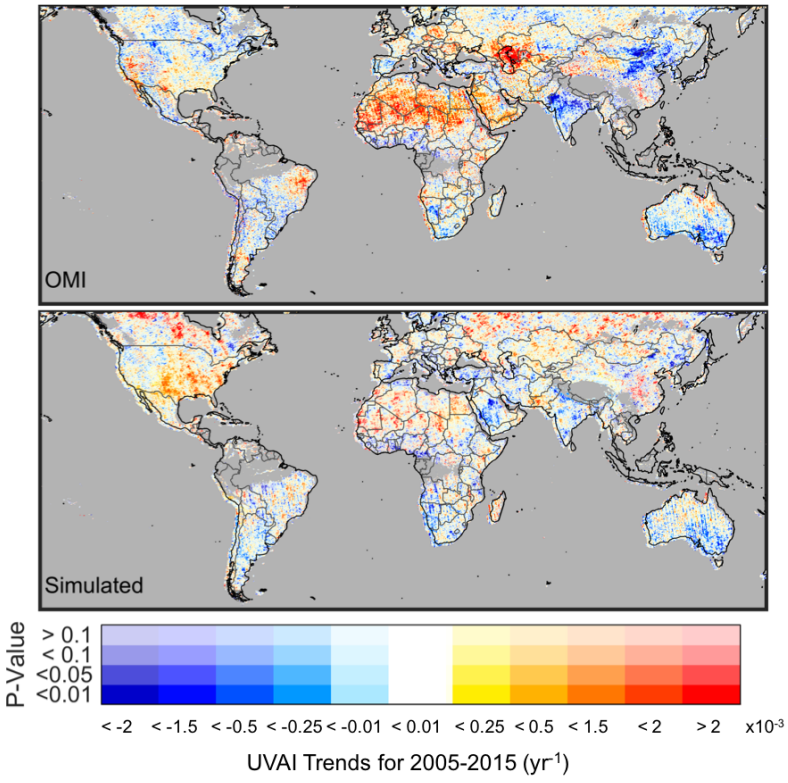

787

788 **Figure 4:** Trends in OMI (top panel) and simulated (bottom panel) UVAI values coincidently
789 sampled from OMI calculated from the Generalized Least Squares regression of monthly time
790 series values over 2005-2015. The opacity of the colors indicates the statistical significance of the
791 trend. Gray indicates persistent cloud fraction greater than 5%.

Atmos. Chem. Phys. Discuss., https://doi.org/10.5194/acp-2017-1183
Manuscript under review for journal Atmos. Chem. Phys.
Discussion started: 12 February 2018

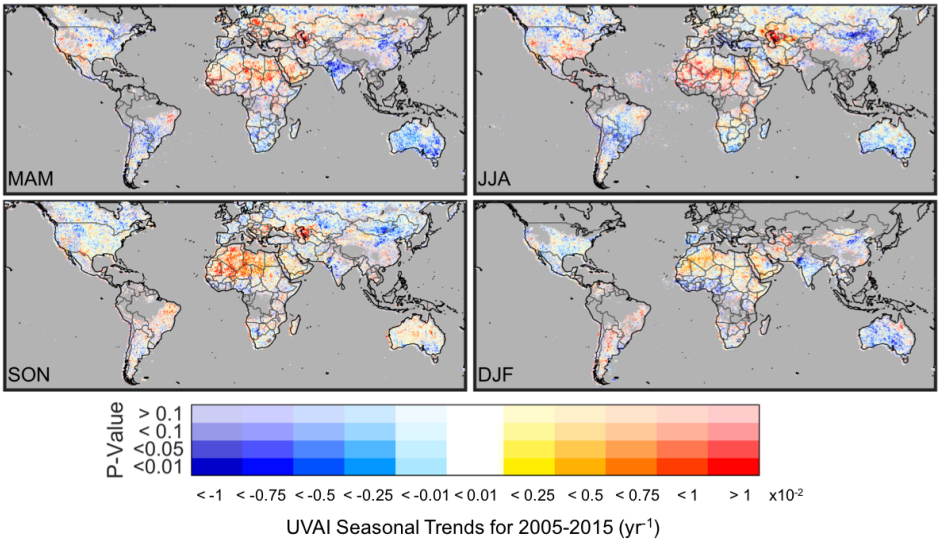

792

793 **Figure 5:** Seasonality of the trends in OMI UVAI values calculated from the Generalized Least
794 Squares regression of monthly time series values over 2005-2015 for MAM (May, April, March),
795 JJA (June, July August), SON (September, October, November), and DJF (December, January,
796 February). The opacity of the colors indicates the statistical significance of the trend. Gray
797 indicates persistent cloud fraction greater than 5%.

Atmos. Chem. Phys. Discuss., https://doi.org/10.5194/acp-2017-1183
Manuscript under review for journal Atmos. Chem. Phys.
Discussion started: 12 February 2018

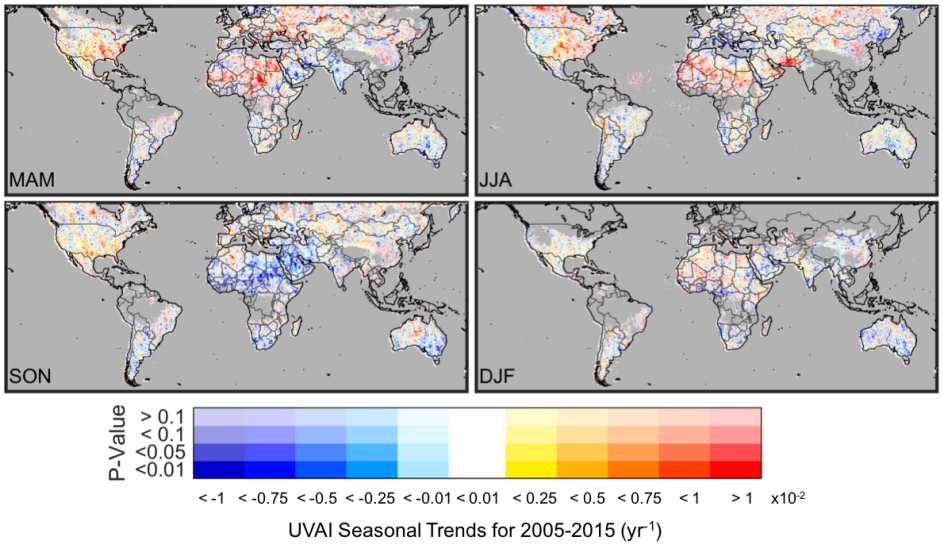

798

799 **Figure 6:** Seasonality of the trends in simulated UVAI values coincidently sampled from OMI
800 calculated from the Generalized Least Squares regression of monthly time series values over 2005-
801 2015 for MAM (May, April, March), JJA (June, July August), SON (September, October,
802 November), and DJF (December, January, February). The opacity of the colors indicates the
803 statistical significance of the trend. Gray indicates persistent cloud fraction greater than 5%.

Atmos. Chem. Phys. Discuss., https://doi.org/10.5194/acp-2017-1183
Manuscript under review for journal Atmos. Chem. Phys.
Discussion started: 12 February 2018

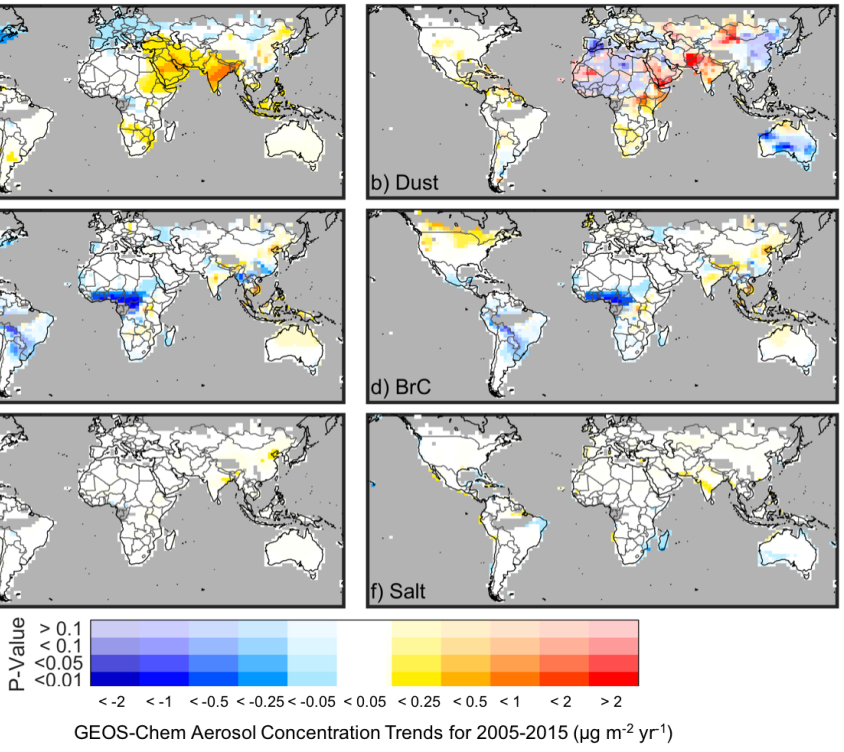

804

805 **Figure 7:** Trend in GEOS-Chem aerosol concentrations for a) secondary inorganic aerosol (SIA),
806 b) dust, c) total organic aerosol (OA), d) brown carbon (BrC), e) black carbon (BC), and f) sea
807 salt. The trends are calculated from the GLS regression of monthly aerosol concentration time
808 series values over 2005-2015. The opacity of the colors indicates the statistical significance of the
809 trend. Gray indicates persistent cloud fraction greater than 5%.

Atmos. Chem. Phys. Discuss., https://doi.org/10.5194/acp-2017-1183
Manuscript under review for journal Atmos. Chem. Phys.
Discussion started: 12 February 2018

Atmospheric Chemistry and Physics Discussions

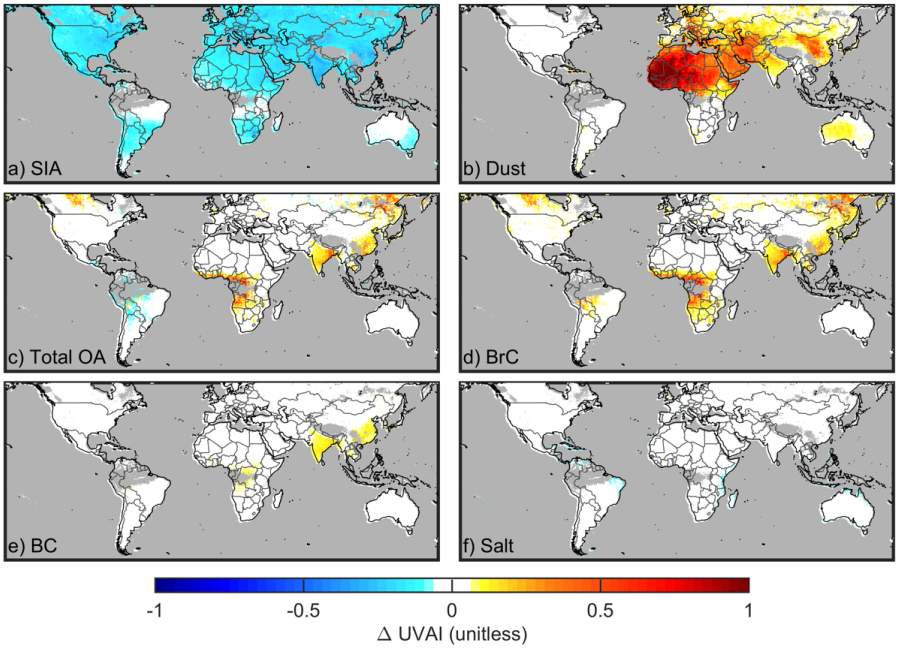

Figure 8: Annual mean change in simulated UVAI values for 2008 due to the doubling of concentrations of a) secondary inorganic aerosol (SIA), b) dust, c) total organic aerosol (OA), d) brown carbon (BrC), e) black carbon (BC), and f) sea salt from the GEOS-Chem simulation. Gray indicates persistent cloud fraction greater than 5%.

Atmos. Chem. Phys. Discuss., https://doi.org/10.5194/acp-2017-1183
Manuscript under review for journal Atmos. Chem. Phys.
Discussion started: 12 February 2018

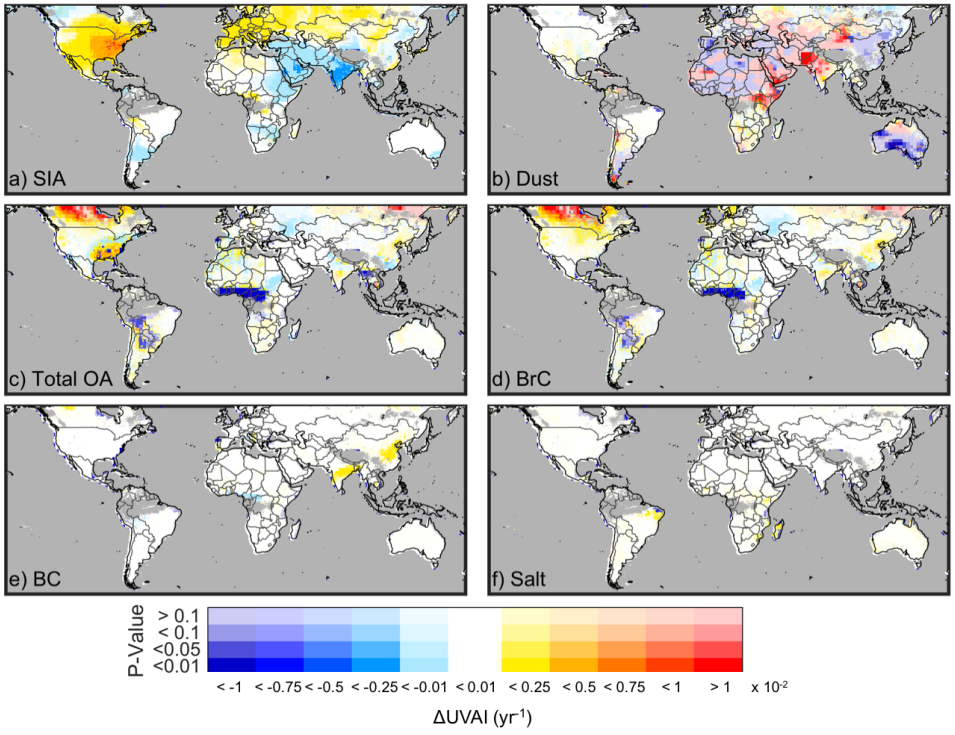

Figure 9: Change in simulated UVAI values due to the 2005-2015 trends in a) secondary inorganic aerosols (SIA), b) dust, c) total organic aerosol (OA), d) brown carbon (BrC), e) black carbon (BC), and f) sea salt from the GEOS-Chem simulation. Gray indicates persistent cloud fraction greater than 5%.